Journal of Structural Geology 33 (2011) 424–432

Contents lists available at ScienceDirect

Journal of Structural Geology

journal homepage: www.elsevier.com/locate/jsg

A Mohr circle method for 3D strain measurement using the geometry of no finite longitudinal strain and the R_{XZ} strain ratio

Khalil Sarkarinejad*, Babak Samani, Ali Faghih

Department of Earth Sciences, College of Sciences, Shiraz University, Shiraz, Iran

ARTICLE INFO

Article history:
Received 9 October 2010
Received in revised form
25 November 2010
Accepted 6 December 2010
Available online 10 December 2010

Keywords:
Strain
Deformed conglomerate
No finite longitudinal strain
Zagros
Iran

ABSTRACT

This paper proposes a new method for 3D finite strain analysis. This method utilizes a Mohr circle construction combined with stereographic projection of the geometry of no finite longitudinal strain and with the strain ratio on the *XZ*-plane of the finite strain ellipsoid. The method is described using numerical examples and then it is tested by applying it to the deformed Deh Vazir conglomerate in the southwestern part of the Sanandaj-Sirjan HP-LT metamorphic belt, within the Zagros orogenic belt in Iran. The results of this method compare well with previous finite strain measurements using strain ratios on three principal planes of finite strain. Calculation of finite strain from strain ratios on the *XY* and *YZ* principal planes is advantageous when preparation of 3 perpendicular sections is difficult or impossible.

1. Introduction

Measurements of finite strain and determination of the strain ellipsoid in naturally deformed rocks are important tasks for many structural geologists. The key to strain analysis lies in finding objects with known initial packing arrangement or features which enable final lengths or angles to be calculated. Following the classic paper of Cloos (1947), a diversity of methodologies has been proposed in order to estimate finite strain in deformed rocks. The R_f/Φ method (Ramsay, 1967; Dunnet, 1969) and Fry method (Fry, 1979) are the most common methods that have been used by structural geologists; they use the shape (R_f/Φ method) and distribution (Fry method) of objects (e.g. deformed ooids, pebbles of deformed conglomerate and deformed fossils) or of points (e.g. quartz grain centers in quartzite). Two dimensional finite strain can be completely described by three numbers which represent the orientations and magnitudes of the strain ellipse. Strain magnitude can be expressed as two principal stretch values, or a strain ratio and area change. For a full description of homogeneous 3D finite strain, six numbers are needed: three to describe the orientation of the strain ellipsoid, and three to describe strain magnitude. Strain magnitude can be expressed by the three principal stretch values, or by two strain ratios and volume change. Ramsay and Huber (1983, p. 198) suggested four approaches that can be used to determine the 3D geometry of the strain ellipsoid from 2D strain ellipse data, among which the approach using two strain ellipses parallel to the principal planes is the most practical. This paper proposes a new method combining stereographic projection of orientations of no finite longitudinal strain together with the principal strain ratio on the *XZ*-plane and using a Mohr circle construction; the method allows one to determine R_{XY}, R_{YZ} (strain ratio in the *XY* and *YZ* principal planes of the strain ellipsoid) and the geometry of the 3D strain ellipsoid. This method is applied to a deformed conglomerate to show how the finite strain varies on a variety of scales across a deformed area.

2. Geometry of no finite longitudinal strain

There are five main types of strain ellipsoid which can result from homogeneous deformation with no volume change (Flinn, 1962). Within the strain ellipsoid, lines whose deformed lengths are equal to their undeformed lengths are defined as lines of no finite longitudinal strain (n.f.l.s) (Ramsay, 1967). Orientations of all lines of no finite longitudinal strain define a surface separating sectors of positive and negative longitudinal strain within the ellipsoid. Except for the plane strain state where the strain ellipsoid shape (k) = 1 which produces two circular sections, this surface is a double cone (on a circular or elliptical base) with common apices at the center of the ellipsoid. The shape of these conical surfaces can be completely described by the angles made by their lines of intersection on the principal planes and one of the principal strain axes (Φ_{XY}, Φ_{XZ}, Φ_{YZ}) (Fig. 1a). The values of

* Corresponding author. Tel.: +98 711 8321348; fax: +98 711 22844572.
E-mail address: Sarkarinejad@geology.susc.ac.ir (K. Sarkarinejad).

0191-8141/$ – see front matter
doi:10.1016/j.jsg.2010.12.002

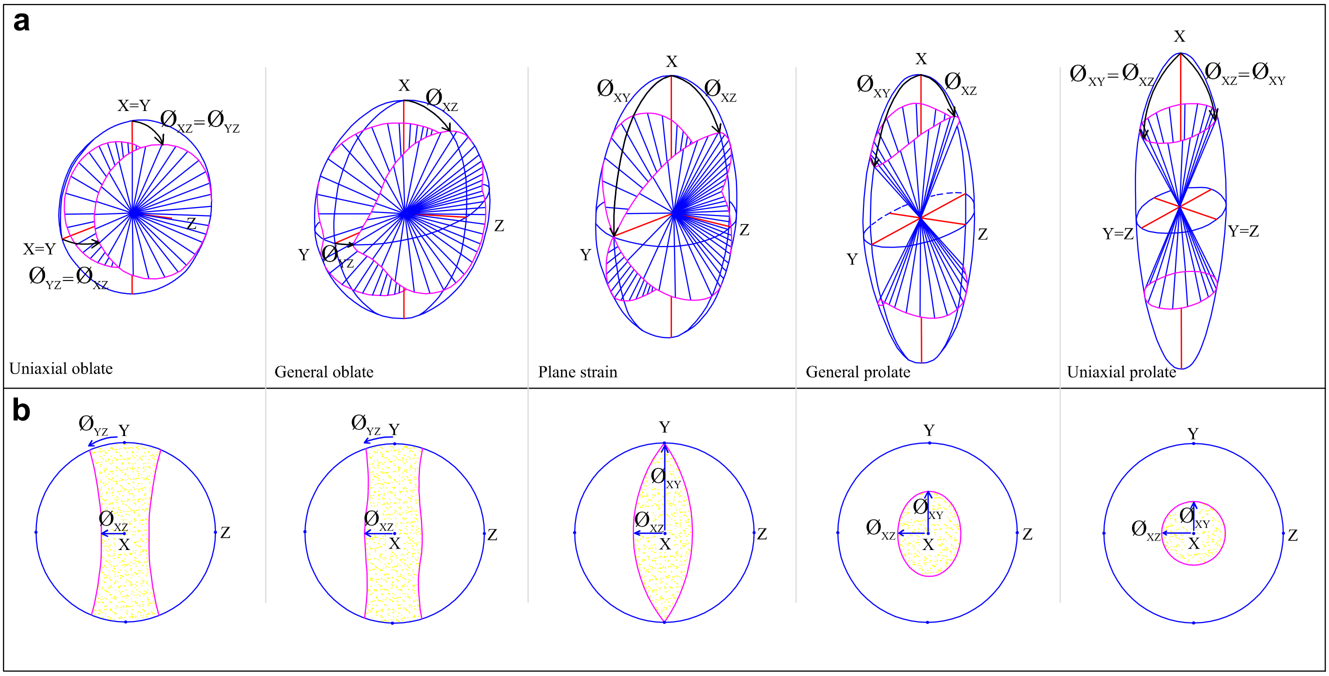

Fig. 1. (a) Geometry of surfaces ($k \neq 1$) and plane ($k = 1$) of no finite longitudinal strain (n.f.l.s) in the five main types of the strain ellipsoid (Ramsay, 1967). (b) Half the maximum and minimum angular dimensions of either the extension field or shortening field are measured on a stereographic projection.

these angles depend upon the principal extensions. Half the maximum and minimum angular dimensions of either the extension field or shortening field are measured on a stereographic projection (Fig. 1b). For an oblate ellipsoid, these are measured from *X* in the *XZ*-plane (Φ_{XZ}) and from *Y* in the *YZ*-plane (Φ_{YZ}) so that Φ_{XZ} is always greater than Φ_{YZ}, unless the oblate ellipsoid is uniaxial ($k = 1$), when $\Phi_{XZ} = \Phi_{YZ}$. For a prolate ellipsoid, the angular dimensions of the extension field are measured from *X* in the *XZ*-plane and designated Φ_{XZ}, and from *X* in the *XY*-plane and designated Φ_{XY}. These angles are equal for a uniaxial prolate ellipsoid, whereas $\Phi_{XY} > \Phi_{XZ}$ for a triaxial prolate ellipsoid. The surface of no finite longitudinal strain is dependent on volume change; the two limits occur when the original sphere either lies completely outside or completely within the strain ellipsoid. Combining a study of deformed structures which have suffered elongation or compression (such as foliation, stretching lineation, boudins and folds) with stereographic analysis of the extension and compression directions will enable us to determine the pattern of no finite longitudinal strain. Comparing results of stereographic analysis with the no finite longitudinal strain pattern on a Flinn diagram (Flinn, 1962; Ramsay and Huber, 1983) provides a qualitative test for determining the homogeneity of strain. If the compression and extension domains are separated by irregular boundaries, the strain has been inhomogeneous. In such cases it is often possible to use data from smaller or larger domains to establish empirically the scale of any domains of homogeneous strain. Large bodies of inhomogeneously strained rock may be divided into volumetric units which are small enough to be considered to have deformed homogeneously (Talbot, 1970; Twiss and Moores, 1992). Similarly small domains of homogeneous strains may integrate within larger domains of homogeneous strains (Talbot, 1987; Talbot and Sokoutis, 1995).

2.1. The Mohr diagram for strain

Nadai (1950) first applied a Mohr circle to represent strain. Nadai recognized that a graph of λ' (reciprocal quadratic elongation) vs γ' ($\gamma' = \gamma/\lambda$ or shear strain/quadratic elongation), in terms of angles in the strain state, is identical in form with the Mohr stress diagram: the three principal planes of the strain ellipsoid are represented by three Mohr circles. The strain state for any other direction falls in the region bounded by the three circles. It was probably Brace (1961) who first used the expression "Mohr diagram" in the geological literature for the representation of three-dimensional finite strain. Ramsay (1967) expanded the usage of the Mohr diagram for strain in two ways. First, he illustrated the potential of Mohr circles for representing strain data. Second, he illustrated how the diagram for three-dimensional reciprocal strain could be used to calculate strain values. For five ellipsoid examples, Ramsay (1967) derived strain contours which were plotted on stereographic projections. In practice, it is more convenient to represent three-dimensional strain on a half Mohr diagram with three semicircles, thus representing the values, but not the sign, of γ'. Usually determination of the strain ellipsoid shape is possible by using the popular *K* factor (Flinn, 1962), where:

$$K = \left[(\lambda_1/\lambda_2)^{1/2} - 1\right] \Big/ \left[(\lambda_2/\lambda_3)^{1/2} - 1\right]$$

$K = 1$ (plane strain ellipsoid, type 3); $K = 0$ (uniaxial oblate ellipsoid, type 1); $K = \infty$ (uniaxial prolate ellipsoid, type 5); $0 < K < 1$ (three axial oblate ellipsoid, type 2) and $1 < K < \infty$ (three axial prolate ellipsoid, type 4). The Mohr diagrams are also a useful means of illustrating and classifying strain ellipsoids of different types. The relationship of the ψ_{max} (maximum shear angle) tangents to the three circles allows ellipsoids to be assigned to one of Ramsay's five equal volume ellipsoid types (Fig. 2). The plane strain ellipsoids are immediately distinguishable with their $\lambda'_1\ \lambda'_2$ and $\lambda'_2\ \lambda'_3$ circles which share the same ψ_{max} line (Fig. 2c). The two end-member ellipsoids, uniaxial prolate ($K = \infty$) and uniaxial oblate ($K = 0$), are represented on the Mohr diagram by a single circle (Fig. 2a and e). In each case, one principal circle reduces to a point and the ψ_{max} is only defined in the *XZ* principal plane of the strain ellipsoid. In the three axial oblate and prolate ellipsoids there are different ψ_{max} for all principal planes of the strain ellipsoid (Fig. 2b and d).

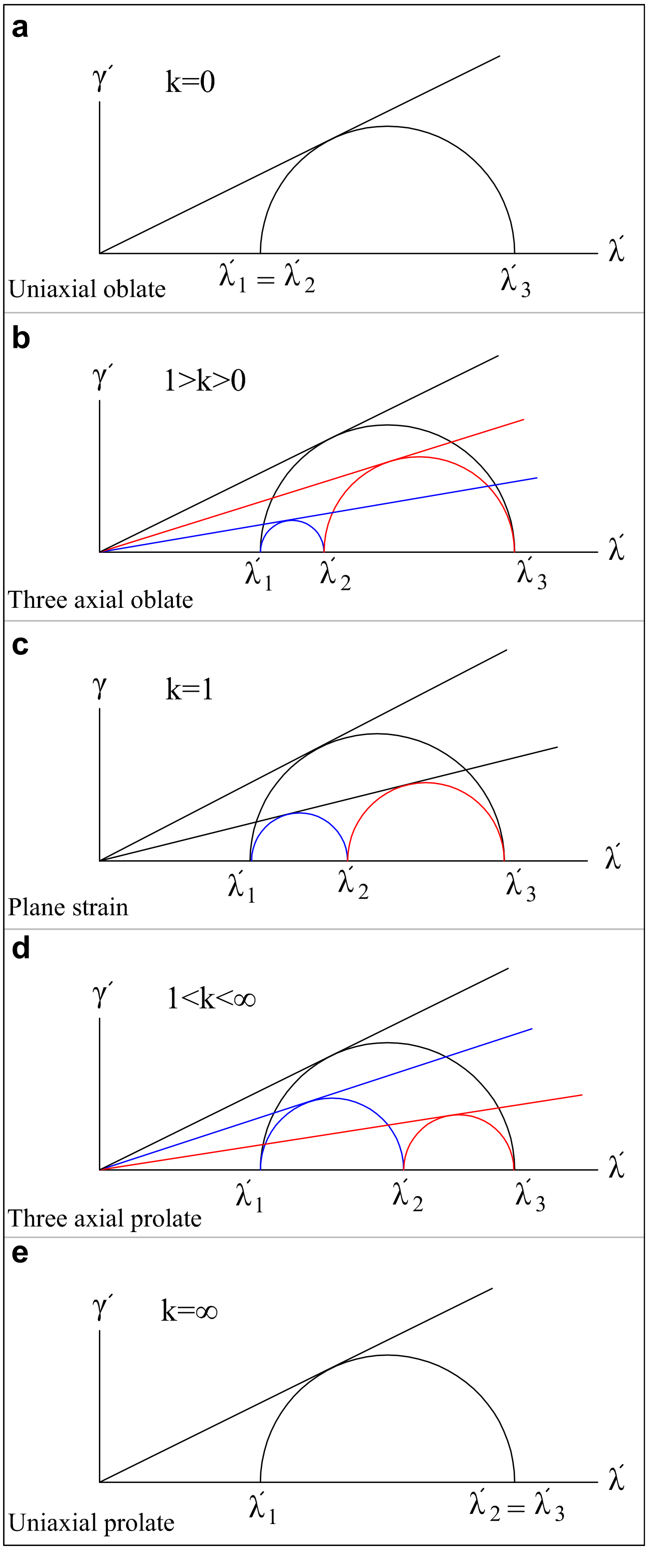

Fig. 2. The relationship of the ψ_{max} tangents to the three principal circles allows strain ellipsoids to be assigned to one of Ramsay's five equal volume ellipsoid types.

2.2. Numeric example

Let us suppose that the data in Table 1 show the strain ratio in the XZ-plane of the strain ellipsoid and the Φ angles obtained from strain analysis and structural studies in three geological settings. It is possible to determine the strain ratio in the other two principal planes (R_{XY} and R_{YZ}) by using a Mohr circle construction. The data of Table 1 were used to calculate the strain ratio in the XY- and YZ-planes for states 1 to 3, respectively. In the first case the values of Φ indicate an oblate geometry for the strain ellipsoid. To measure the strain ratio in the other two principal planes based one a Mohr circle construction, the following steps are used. Draw perpendicular axes $c\lambda'$ and $c\gamma'$, where c is a constant of unknown value (Fig. 3a). For strain analysis of naturally deformed rocks, because it is rare to know the original size of the strain markers, we can only determine the relative strain ratios of the principal planes of finite strain ellipsoid but not the absolute strain ratios (Twiss and Moores, 1992). So we can use an arbitrary scale or unit for the quadratic elongation (λ') axis, as proposed by Ramsay (1967). By determining the position of $\lambda' = 1$ on the λ' horizontal axis we can obtain a numerical scale for determination of other strain parameters. Construct a Mohr circle with center C and radius $R_{XZ}/2$. The two points where this circle cuts the λ'-axis represent the two principal axes of the strain ellipsoid. At λ'_3 construct a line making an angle $\Phi_{XZ} = 35°$ (Table 1) with the λ'-axis. This line cuts the Mohr circle at the point m. Drop a perpendicular from m onto the λ'-axis, intersecting it at n. This line shows the locus of no finite longitudinal strain (n.f.l.s) and cuts the λ'-axis at $\lambda' = 1$. For the plane strain ellipsoid ($k = 1$), the n.f,l.s. locus is a circular section. In all other cases ($k \neq 1$), the two loci do not coincide and the locus of n.l.f.s. represents a surface, not a plane. Then at λ'_3 construct a line making an angle $\Phi_{YZ} = 20°$ with the λ'-axis so it cuts the mn line (Fig. 3a–c) at o. The intersection of these lines is located in the YZ principal plane of the strain ellipsoid. Because λ'_3 and o lie on the circumference of $\lambda'_2\,\lambda'_3$ principal plane, the line $o\lambda'_3$ is a chord of that circle, and its perpendicular bisector intersects the λ'-axis at the center of the $\lambda'_2\,\lambda'_3$ circle in Mohr space. The XY principal plane can be easily determined by constructing a circle with a radius of $\lambda'_1\lambda'_2/2$. The magnitude of the principal quadratic elongations λ'_1, λ'_2 and λ'_3 can be found by scaling off the distance from the origin; hence:

$$\lambda'_1 = \frac{c\lambda'_1}{cn}\quad \lambda'_2 = \frac{c\lambda'_2}{cn}\quad \lambda'_3 = \frac{c\lambda'_3}{cn}$$

The second case in Table 1 is for a prolate strain ellipsoid. Construct the Mohr circle with center C and radius $R_{XZ}/2$ (Fig. 3b). From the minimum principal quadratic elongation (λ'_3) construct a line making an angle $\Phi_{XZ} = 30°$ with the λ'-axis. As in the previous case, this line cuts the Mohr circle at m. Drop a perpendicular from m onto the λ'-axis, intersecting it at n. The line mn cuts the λ'-axis at $\lambda' = 1$. Construct an angle 90-Φ_{XY} from λ'_1 so that it cuts the line of n.f.l.s (or mn) at o. Because it is not possible to find the position of λ'_2 on the λ'-axis, it is necessary to use the 90-Φ_{XY} angle for constructing $\lambda'_1\,\lambda'_2$ on the circle. The line $o\lambda'_1$ is a chord of the $\lambda'_1\,\lambda'_2$ circle and its perpendicular bisector intersects the λ'-axis at the center of the $\lambda'_1\,\lambda'_2$ circle (q). With this center (q) and the radius $q\lambda'_1$, one can draw the $\lambda'_1\,\lambda'_2$ circle. Then applying the above equations, it is possible to determine the strain ratios in the XZ, XY and YZ principal planes.

The third case (Table 1) is for a strain ellipsoid with plane strain geometry. All states in this case are the same as that described for

Table 1
Numerical data for three cases showing the strain ratio in the XZ-plane of the strain ellipsoid and Φ_{XY}, Φ_{XZ}, Φ_{YZ} angles. Incomplete data are assumed: in each case it is assumed that one of the angles, Φ_{XY}, Φ_{XZ} and Φ_{YZ}, is missing.

	R_{XZ}	Φ_{XZ}	Φ_{XY}	Φ_{YZ}
Case 1	2	35	–	20
Case 2	2	30	40	–
Case 3	2	40	90	–

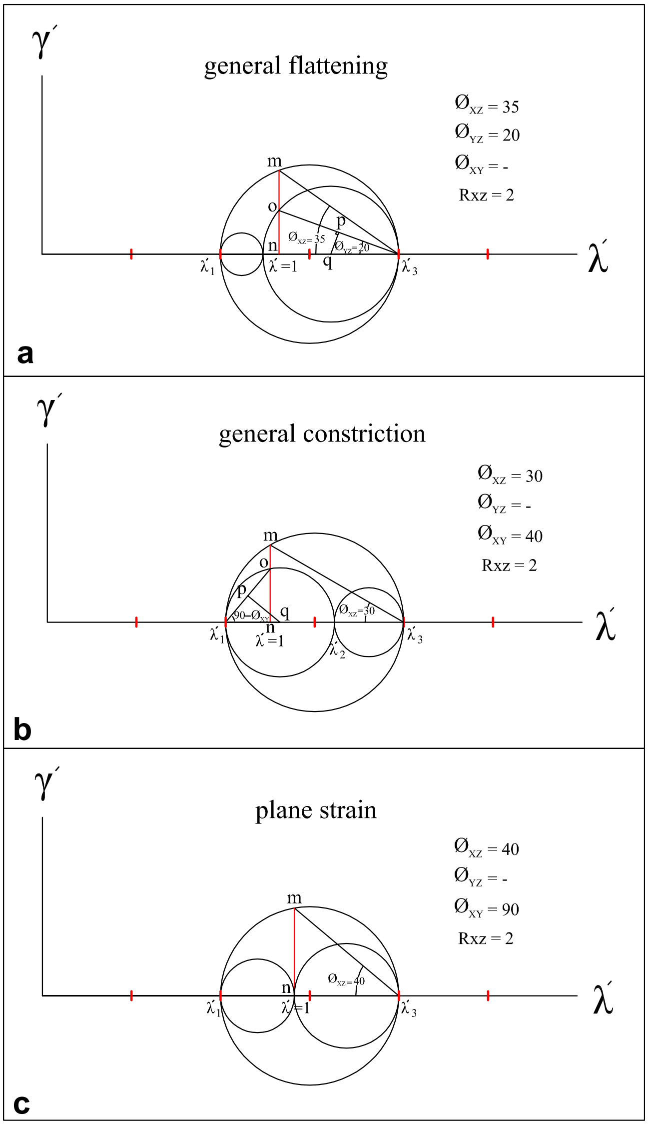

Fig. 3. Measuring the strain ratio in R_{XY} and R_{YZ} principal planes based on Mohr circle construction with application of the geometry of n.f.l.s and the R_{XZ} strain ratio for general flattening (a), general constriction (b) and plane strain (c).

constrictional strain and use the 90-Φ_{XY} angle for constructing the λ'_1 λ'_2 circle (Fig. 3c). In the cases of uniaxial flattening and constriction, the angle $\Phi_{YZ} = \Phi_{XZ}$ and $\Phi_{XY} = \Phi_{XZ}$ and because $\lambda'_2 = \lambda'_1$ and $\lambda'_3 = \lambda'_2$, calculating the strain ratios in the *XY*- and *YZ*-planes can be done based on the strain ratio in *XZ*-plane.

3. Practical applications: regional geological background

Deformed conglomerate and metamorphic rocks of the Deh Vazir area in southwestern Iran (Fig. 4a and b) form part of the Sanandaj-Sirjan metamorphic zone (Stöcklin, 1968), within the Zagros orogenic belt of Iran. The Zagros belt, as part of the Himalayan mountain chain, extends for about 2000 km in a NW–SE direction from the East Anatolian fault of Eastern Turkey to the Oman line in southern Iran (Alavi, 1994). The Zagros Orogen formed by continental collision between the Afro-Arabian continent and the Iranian microcontinent in Late Cretaceous to Tertiary time (Berberian and King, 1981). The orogenic belt is the result of closure of Neo-Tethys by consumption of oceanic crust at a NE-dipping subduction zone below the Iranian microcontinent and subsequent Late Cretaceous continental collision between the Afro-Arabian continent and Iranian microcontinent (Ricou, 1971; Takin, 1972; Dewey et al., 1973; Stocklin, 1968; Berberian and King, 1981; Alavi, 1994; Blanc et al., 2003; McQuarrie, 2004; Sarkarinejad et al., 2008; Sheikholeslami et al., 2008). The Zagros orogenic belt from northeast to southwest consists of three NW–SE trending parallel zones (Fig. 4a): (1) the UrumiehDokhtar Magmatic Belt (UDMB). (2) the Sanandaj-Sirjan HP-LT/HT-LP Metamorphic Belts (SSMB) and (3) the Zagros Fold-and-Thrust Belt (ZFTB). The Sanandaj-Sirjan HP-LT is 150–200 km wide and more than 1500 km long from NW (Sanandaj) to SE (Sirjan) in the western part of Iran (Fig. 4a). Based on metamorphic grade, the Sanandaj-Sirjan zone is subdivided into high-pressure/low temperature and high temperature/low pressure paired metamorphic belt (Sarkarinejad, 1999). The tectonics of the Sanandaj-Sirjan HP-LT metamorphic belt are characterized by numerous thrusts, all transporting rock units from NE to SW in piggyback style (Alavi, 1994).

The results $^{40}Ar/^{39}Ar$ step-heating measurements on biotite, muscovite and amphibole in the Sanandaj-Sirjan HP-LT metamorphic belt are consistent with the overprinting relationship determined from field observations (Sarkarinejad et al., 2009). The first generation of biotite yields plateau ages of 119.95 $\pm$ 0.88 and 112.58 $\pm$ 0.66 Ma. These late Aptian ages are related to early thrusting and the formation of high-pressure metamorphic rocks at the peak of metamorphism prior to obduction of the Neyriz ophiolite (Sarkarinejad et al., 2009). The Deh Vazir deformed conglomerate is sandwiched between thrust sheets which are part of the Zagros Thrust System (Sarkarinejad and Azizi, 2008; Sarkarinejad et al., 2010), which consists of eight sheets of NW-striking, NE-dipping dextral strike-slip duplex structures that are linked with imbricate fans and oblique slip thrusts (Sarkarinejad and Azizi, 2008).

The most abundant rocks in the study area are deformed conglomerate and micro-conglomerate. The conglomerate pebbles consist of quartzite, phyllite, mica schist; the thickness of this unit varies between 2300 and 2500 m. The matrix around the pebbles is composed of muscovite, quartz, and feldspar. The similarity of composition between pebbles and matrix indicates low rheological contrast between them (Sarkarinejad et al., 2010). The metamorphic grade in this conglomerate is greenschist facies conditions (Sarkarinejad, 1999, 2007).

3.1. Meso- and micro-scale structures

The Deh Vazir conglomerate is strongly foliated and lineated (Fig. 5). The foliation is defined by alignment of pebbles flattened in the *XY*-plane. The orientation of the foliation varies between N80°W, 30°NE and N30°W, 70°NE. The stretching lineation within the foliation has a plunge and trend varying from 10°, N60°W to 30°, N20°W. Stair-stepping structures, mantled σ-type porphyroclast systems with sigmoidal structures, asymmetrical rotated domino boudins, asymmetrical tapering boudins and asymmetrical complex rotated domino and tapering boudins all indicate a top-to-the-SE sense of shear (Fig. 6).

3.2. Structural observations and finite strain analysis

Detailed structural observations and sampling for strain analysis were carried out along a narrow (1 km) section across the thrust faults (Fig. 4). Five structural domains (D1 to D5) with different structural characteristics are defined based on distance from thrust faults (Fig. 7). In each domain an oriented sample was taken for strain analysis and more than 60 foliation and stretching lineation measurements were made for stereographic studies. In strain studies the evidence for volume change is commonly equivocal (Simpson, 1981; Mohanty and Ramsay, 1994), but in some cases, volume change can be discounted (Srivastava et al., 1995;

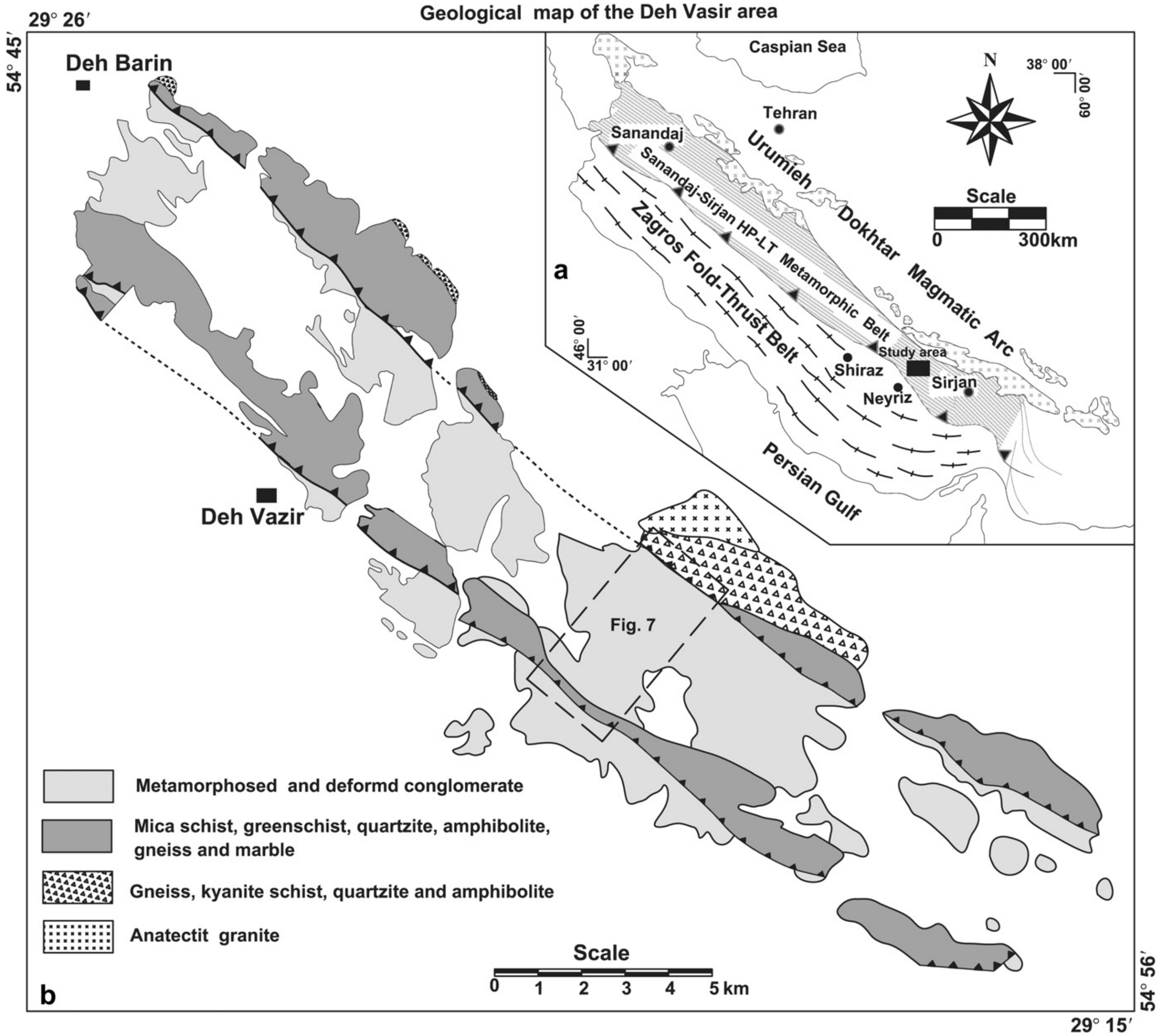

Fig. 4. Geological map of the study area.

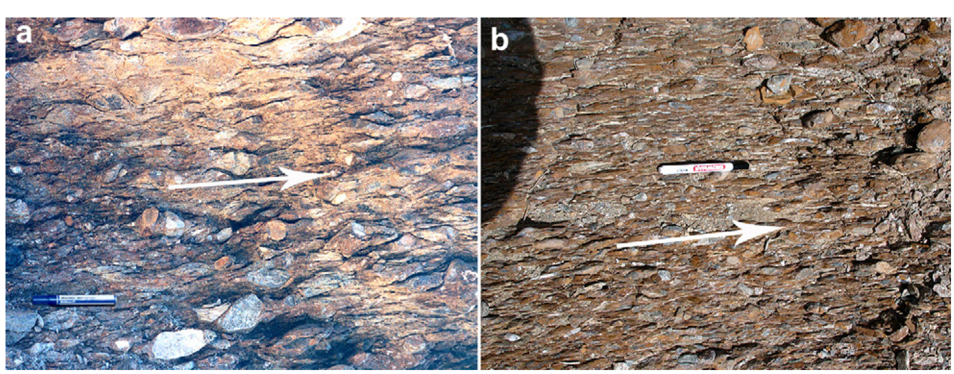

Fig. 5. Preferred orientation of pebble long axes in the Deh Vazir deformed conglomerate. Size of the markers on the left and center of the photos (a and b) is 14 cm. The orientation of the long axes of the pebbles is 10°, N60°W (The photos have been taken looking at inclined faces approximately parallel to the *XZ*-plane of the finite strain ellipsoid).

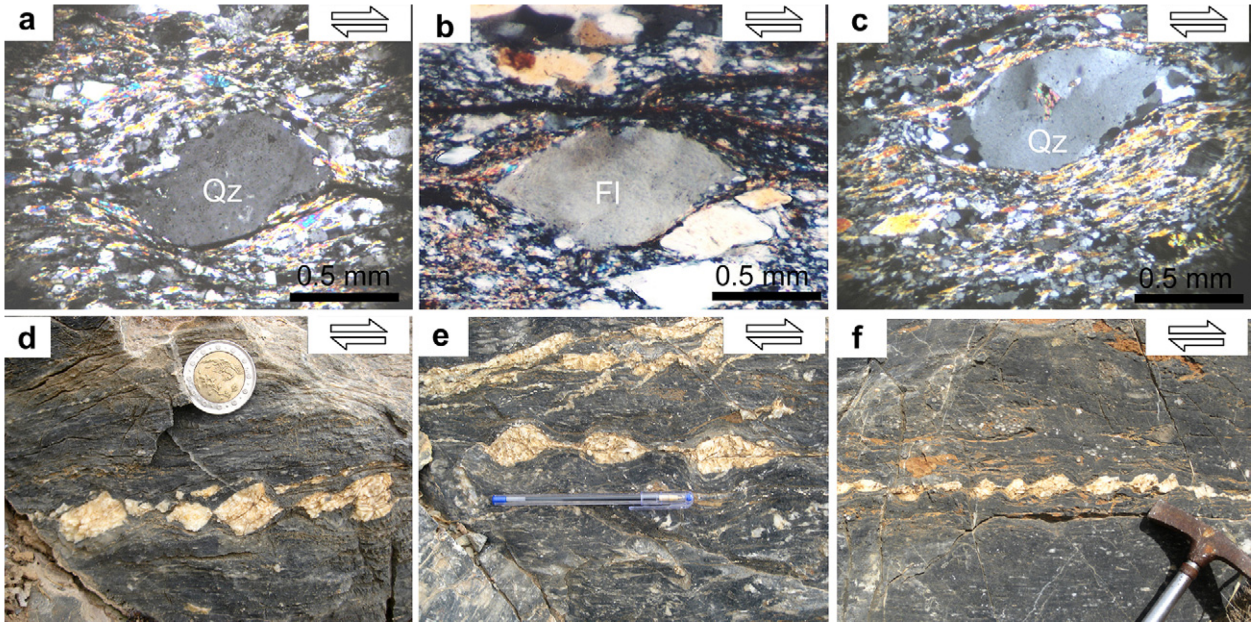

Fig. 6. Shear sense indicators in the study area. (a, b and c) Photomicrographs showing dextral shear of quartz and feldspar σ-type porphyroclast systems. The matrix consists of muscovite, quartz and feldspar. (d) Dextral asymmetrical rotated domino boudins. (e) Asymmetrical tapering boudins. (f) Asymmetrical complex domino and tapering boudins.

Bhattacharyya and Huddleston, 2001). Volume change during deformation can affect the shape of the finite strain ellipsoid (Ramsay and Wood, 1973). In the Deh Vazir deformed area, the lack of prominent veining implies that volume change was small (Sarkarinejad et al., 2010). In the quartzite pebbles, crystal-plastic deformation was dominant as indicated by subgrain-rotation recrystallization microstructures (Sarkarinejad and Azizi, 2008) and there is little or no microstructural evidence for solution transfer, also indicating approximately constant volume deformation. Previous strain studies in this area (Sarkarinejad, 2007; Sarkarinejad and Azizi, 2008) on the deformed conglomerates and micro fossils of the Sanandaj-Sirjan HP-LT metamorphic belt approximately show the plane strain geometry of finite strain ellipsoid ($K \approx 0.85$) with only small volume changes. Quartz c-axis fabrics are type-I crossed-girdle patterns, which indicate approximately plane strain ($K = 1$) conditions (Sarkarinejad and Azizi,

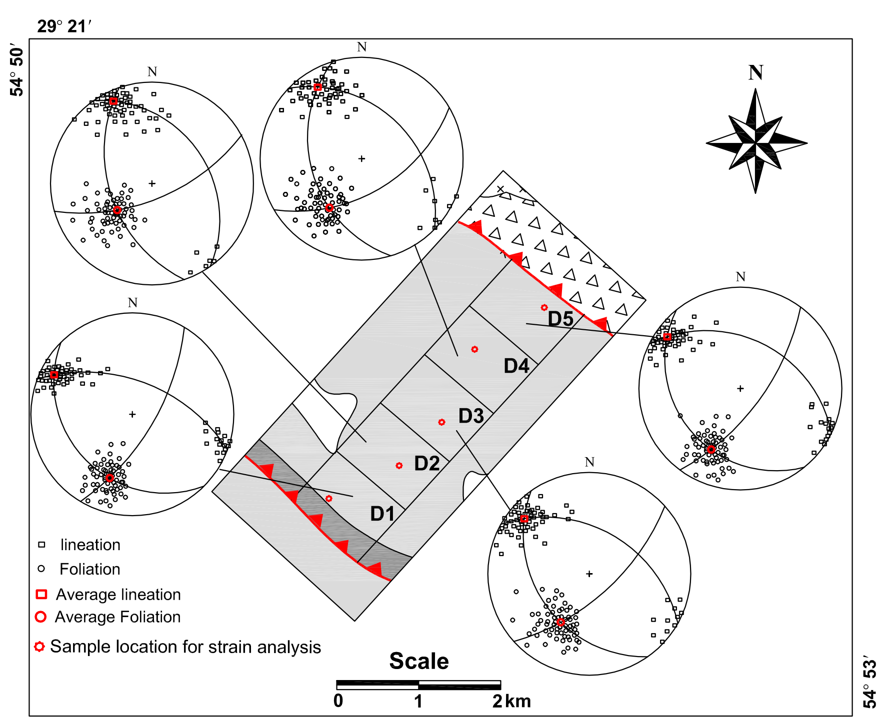

Fig. 7. Five structural domains (D1 to D5), sample locations and distribution of foliation and lineation on lower hemisphere equal area stereographic projections using SpheriStat 2.2 software.

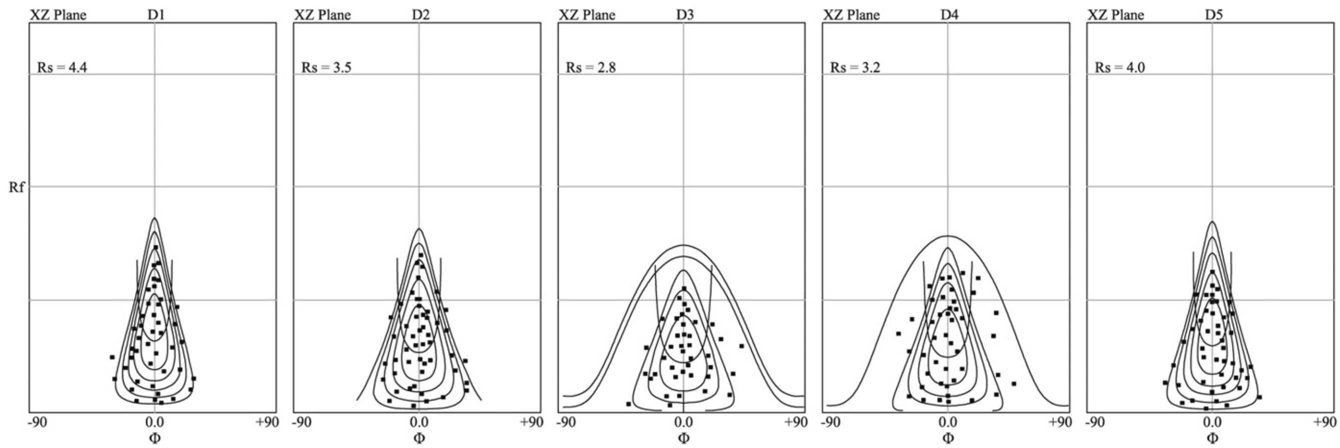

Fig. 8. *Rf*/*Φ* diagrams in the *XZ*-plane for B1 to B5 samples.

2008; Sarkarinejad et al., 2010). Therefore throughout this analysis, we have assumed constant volume deformation.

As mentioned by Xypolias (2009), the kinematic vorticity parameter (W_m) plays an important role in determining the orientation of the principal axes of the finite strain ellipsoid with respect to the instantaneous stretching axes (ISA). Kinematic vorticity is a dimensionless measure of rotation relative to strain and characterizes the amount of shortening relative to displacement. W_m was originally defined as an instantaneous rotation relative to the instantaneous stretching at a point (Truesdell, 1953; Means et al., 1980). Most of the vorticity methods utilize data collected on the *XZ*-plane of finite strain (parallel to lineation and normal to foliation) and commonly assume steady-state deformation with the vorticity vector approximately parallel to the *Y*-axis of the strain ellipsoid.

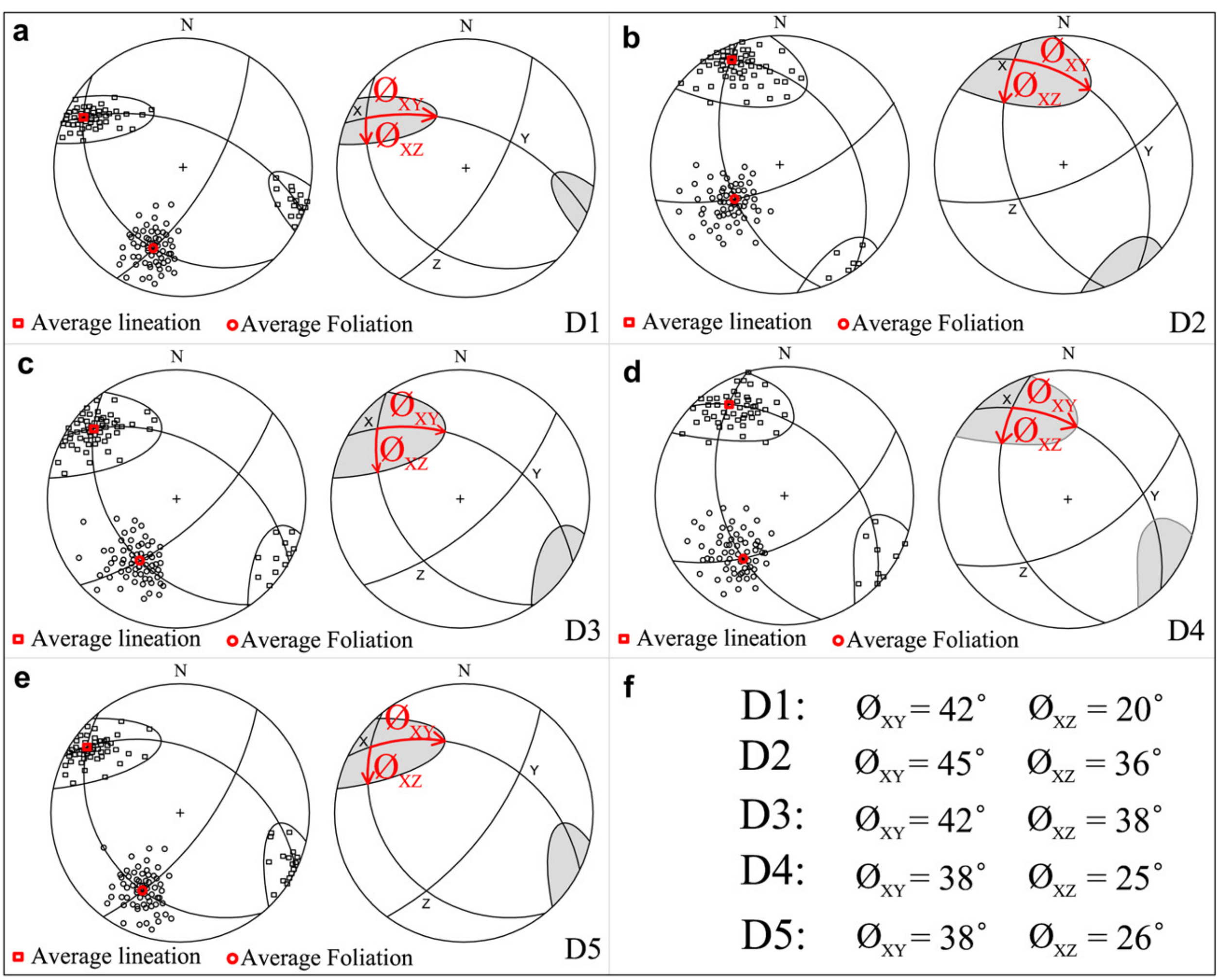

Fig. 9. Lower hemisphere, equal area projection of the n.f.l.s geometry (Φ_{XY} and Φ_{XZ}) based on foliation and stretching lineation structural elements (The stereonets have been plotted using SpheriStat 2.2 software).

Table 2
Strain ratios on the *XY* and *YZ* principal planes of the strain ellipsoid.

	R_{XZ}	Φ_{XZ}	Φ_{XY}	R_{XY}	R_{YZ}
D1	4.4	20°	42°	4.2	3.5
D2	3.5	36°	45°	3.3	2.9
D3	2.8	38°	42°	2.8	2.6
D4	3.2	25°	38°	2.7	2.4
D5	4.0	26°	38°	2.8	2.5

For cases of simple shear and sub-simple shear, W_m is measured on a scale between 0 and 1, with 0 being pure shear and 1 being simple shear. The W_m scale is not linear, but can be converted to a linear scale by considering the percent of a deformation resulting from simple shear and pure shear. Fort and Bailey (2007) propose three separate fields for pure, general, and simple shear dominated deformations. Pure shear dominated deformations have W_m-values of 0–0.3, corresponding to less than 20% simple shear. In contrast, simple shear dominated deformations have W_m-values of greater than 0.95, corresponding to greater than 80% simple shear. General shear occupies the range between 0.3 and 0.95.

W_m is an important factor indicating fit or discord of principal axes of the finite strain ellipsoid and the instantaneous stretching axes of deformation. In pure shear dominated deformation, the maximum and minimum instantaneous stretching axes (ISA_1 and ISA_2) approximately coincide with the short and long axes of the finite strain ellipse (Passchier and Trouw, 2005; Xypolias, 2009) and the deformation is mainly coaxial. In this case the pole of foliation and orientation the stretching lineation show the directions of shortening and extension, respectively. Kinematic vorticity analysis of the Deh Vazir deformed area revealed a prominent pure shear component of deformation (Sarkarinejad et al., 2010; Samani, 2010). So in this study we assumed that the shortening and extension directions approximately coincide with the pole to foliation and the stretching lineation, respectively. Moreover in this framework we can use other structures such as fold axial planes and boudin necks for separation of shortening and extension domains (Talbot, 1970).

Strain analysis was performed on a representative sample from the deformed conglomerate in each of the 5 domains (D1 to D5); sample localities are shown on Fig. 7. All samples were collected from conglomerate layers containing low competency contrast between pebbles and matrix and well defined planar and linear fabric elements. The pebble shape was used as the strain marker. Length-to-width ratios of pebbles were determined from measurements made on sections cut normal to the foliation and parallel to the lineation.

The study relies on the following assumptions: (1) the foliation plane coincides with the *XY*-plane of the strain ellipsoid, (2) the stretching lineation defines the long axis of the strain ellipsoid, (3) the strike of the main thrust faults defines the direction of the shear zone boundaries and ϕ is the angle between the *X*-axis of the elliptical strain marker and the reference line of the shear zone boundary trace and (4) the deformation was isochoric (constant volume). The strain ratios (R_{XZ}) were estimated for each sample applying the R_f/Φ method (Ramsay, 1967; Lisle, 1985) (Fig. 8). In order to determine the 3D geometry of the finite strain ellipsoid, the above described method was used to estimate the tectonic strain ratios in the *XY* and *YZ* principal planes. By applying stereographic analysis of the stretching lineation and foliation, we determined the geometry of the surfaces of n.l.f.s. More than 60 orientations of foliation and stretching lineation were measured at each sample location in the D1 to D5 domains. For each domain the distributions of orientations were plotted on lower hemisphere, equal area stereographic projections (Fig. 7). The orientations of n.l.f.s. were determined. Their geometry can be completely described by the angles made by their lines of intersection on the principal planes and one of the principal strain axes (angles Φ_{XY}, Φ_{XZ}, Φ_{YZ}) (Fig. 9). Finally by using the geometry of n.l.f.s. (angles Φ_{XY}, Φ_{XZ}, Φ_{YZ}) and the tectonic strain ratio on the *XZ*-plane and by applying the method described above, the strain ratios on the *XY*- and *YZ*-planes were calculated (Table 2). These three values of strain (for the *XZ*-, *XY*- and *YZ*-planes) have been used to evaluate the finite natural logarithmic strain (Ramsay and Huber, 1983):

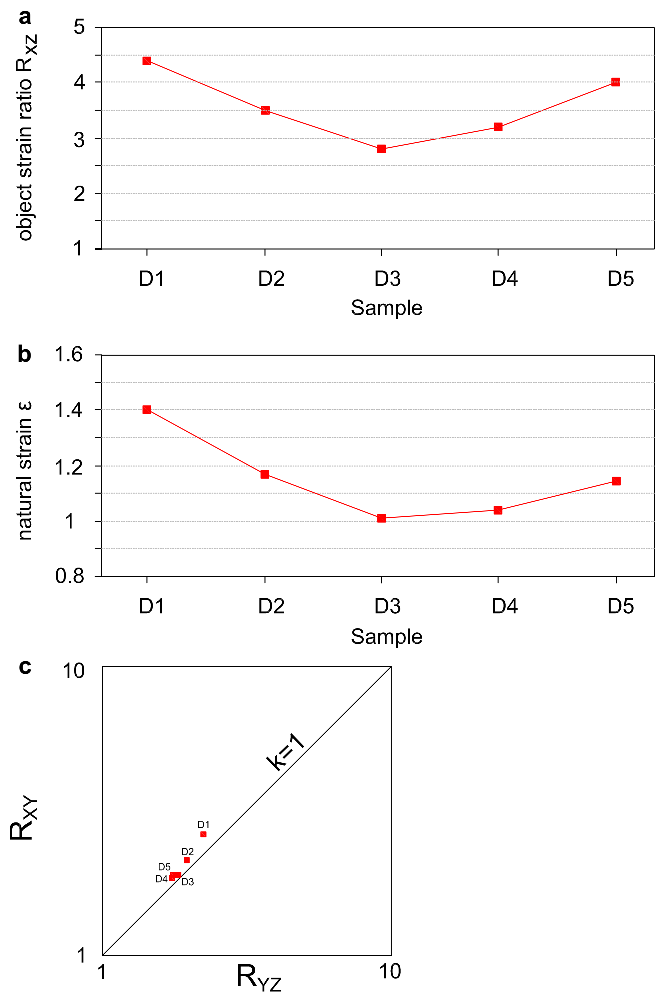

Fig. 10. (a and b) Variation of finite strain parameters (R_{XZ} and ε) plotted against sample locations from the thrust planes. (c) Ellipsoid shape analyzed by plotting the finite strains for *XY* and *YZ* principal sections on a Ramsay diagram.

$$\varepsilon = \left(\frac{1}{3}\right)^{1/2}\left[(\ln(R_{XZ}))^2+(\ln(R_{YZ}))^2+(\ln(R_{XY}))^2\right]^{1/2}$$

In order to investigate the finite strain variation across the shear zones, finite strain parameters (R_{XZ} and ε) were plotted against sample locations from the thrust planes (Fig. 10a and b); for each distribution, curves of mean values have been plotted. The ellipsoid shape was analyzed by plotting the finite strain for the *XY*- and *YZ*-planes on a Ramsay diagram (Fig. 10c).

4. Discussion

The shear zones associated with the Zagros thrust system (Sarkarinejad and Azizi, 2008) are characterized by a top-to-the-SW sense of shear and lengthening parallel to the shear direction. This conclusion is based on two main lines of evidence: (1) the stretching lineation is roughly parallel to the shear direction as obtained by independent field evidence (Fig. 6); and (2) the stretching lineation trend is at a high angle with respect to the general dip direction of the foliation (Fig. 9). *XZ* finite strain values obtained from deformed pebbles, as well as the calculated natural logarithmic strain (ε), indicate that finite strain increases in an approximately linear fashion toward the thrust faults (Fig. 10a and b). Similar linear trends have been observed in other shear zones (Talbot and Sokoutis, 1995). Vitale and Mazzoli (2008) discriminated mylonite types using strain intervals of $\varepsilon = 0–1$ (protomylonites), $\varepsilon = 1–2.5$ (mylonite) and $\varepsilon > 2.5$ (ultramylonite). Our analyzed samples have strain values ($1 < \varepsilon < 1.4$) corresponding to mylonite. The Ramsay diagram (Fig. 10c) shows that most of the object finite strain ellipsoids inferred from the deformed pebbles fall into the prolate field, although they plot close to the plane strain line. The finite strain ellipsoid distribution in the Ramsay diagram is similar to that obtained for the region by applying R_{XZ}, R_{XY} and R_{YZ} strain ratios in planes cut parallel to the finite strain principal planes (Sarkarinejad et al., 2010). Thus both previous methods and the newly described method of finite strain determination give approximately similar values for the study area.

5. Conclusion

3D strain analysis based on the geometry of the surface of no finite longitudinal strain and the strain ratio measured on the *XZ*-plane is a useful method for strain studies in deformed areas with approximately homogeneous deformation. This method is especially useful for situations when preparation of 3 perpendicular cut sections is difficult or impossible.

Acknowledgements

The authors wish to thank Editor of Journal of Structural Geology, Professor Tom G. Blenkinsop who critically reviewed the manuscript and made valuable suggestions for its improvement. We are grateful to Professor Jan Tullis for critical reading of the manuscript, which greatly improved the presentation. Professor C.J. Talbot and anonymous reviewer are thanked for constructive review that has greatly improved the quality of the final version. The research was supported by the Shiraz Research Council (SURC) grant which is gratefully acknowledged.

References

Alavi, M., 1994. Tectonics of the Zagros orogenic belt of Iran: new data and interpretations. Tectonophysics 229, 211–238.
Berberian, M., King, G.C.P., 1981. Towards a paleogeography and tectonic evolution of Iran. Canadian Journal of Earth Sciences 18, 210–265.
Bhattacharyya, P., Hudleston, P., 2001. Strain in ductile shear zones in the Caledonides of northern Sweden: a three-dimensional puzzle. Journal of Structural Geology 23, 1549–1565.
Blanc, E.J.-P., Allen, M.B., Inger, S., Hassani, H., 2003. Structural styles in the Zagros Simple Folded Zone, Iran. Journal of the Geological Society of London 160, 401–412.
Brace, W.F., 1961. Mohr construction in the analysis of large geologic strain. Bulletin of Geoligical Society of America 72, 1059–1080.
Cloos, E., 1947. Oolite deformation in the South Mountain fold, Maryland. Bulletin of Geological Society of America 68, 843–918.
Dewey, J.F., Pitman III, W.C., Ryan, W.B.F., Bonnin, J., 1973. Plate tectonics and the evolution of the Alpine System. Bulletin of Geological Society of America 84, 3137–3180.
Dunnet, D., 1969. A technique of finite strain analysis using elliptical particles. Tectonophysics 7, 117–136.
Flinn, D., 1962. On folding during three-dimensional progressive deformation. Geological Society of London Quarterly Journal 118, 385–433.
Fort, A.M., Bailey, C.M., 2007. Testing the utility of the porphyroclast hyperbolic distribution method of kinematic vorticity analysis. Journal of Structural Geology 29, 983–1001.
Fry, N., 1979. Random point distribution and strain measurements in rocks. Tectonophysics 60, 89–105.
Lisle, R.J., 1985. Geological Strain Analysis: A Manual for the Rf/ϕ Technique. Pergamon Press, Oxford, pp. 99.
McQuarrie, N., 2004. Crustal scale geometry of the Zagros fold-and-thrust belt, Iran. Journal of Structural Geology 26, 519–535.
Means, W.D., Hobbs, B.E., Lister, G.S., Williams, P.F., 1980. Vorticity and non-coaxiality in progressive deformations. Journal of Structural Geology 2, 371–378.
Mohanty, S., Ramsay, J.G., 1994. Strain partitioning in ductile shear zones: an example from a Lower Pennine nappe of Switzerland. Journal of Structural Geology 16, 663–676.
Nadai, A., 1950. Theory of Flow and Fracture of Solids. McGraw-Hill, New York.
Passchier, C.W., Trouw, R.A.J., 2005. Microtectonics. Springer-Verlag, Berlin, pp. 366.
Ramsay, J.G., 1967. Folding and Fracturing of Rocks. McGraw-Hill, New York.
Ramsay, J.G., Huber, M.I., 1983. The Techniques of Modern Structural Geology, 1: Strain Analysis. Academic Press, London.
Ramsay, J.G., Wood, D.S., 1973. The geometric effects of volume change during deformation processes. Tectonophysics 16, 263–277.
Ricou, L.E., 1971. Le croissant ophiolitique pe'ri-arabe. Une ceinture de nappes mises en place au Cre'tace' supe'rieur. Revue de Ge'ographie Physique et de Ge'ologie Dynamique XIII, 327–350 (Paris).
Samani, B., 2010. Finite strain and deformation flow geometry in the Sanandaj-Sirjan HP-LT metamorphic belt, Iran. Ph.D. thesis, Shiraz University, Iran, unpublished.
Sarkarinejad, K., 1999. Tectonic finite strain analysis using Ghuri deformed conglomerate, Neyriz area Southwestern Iran. Iranian Journal of Science and Technology 23, 351–363.
Sarkarinejad, K., 2007. Quantitative finite strain and kinematic flow analyses along the Zagros transpression zone. Iran. Tectonophysics 442, 49–65.
Sarkarinejad, K., Azizi, A., 2008. Slip partitioning and inclined dextral transpression along the Zagros Thrust System, Iran. Journal of Structural Geology 30, 116–136.
Sarkarinejad, K., Faghih, A., Grasemann, B., 2008. Transpressional deformations within the Sanandaj-Sirjan Metamorphic Belt (Zagros Mountains, Iran). Journal of Structural Geology 30, 818–826.
Sarkarinejad, K., Godin, L., Faghih, A., 2009. Kinematic vorticity flow analysis and $^{40}Ar/^{39}Ar$ geochronology related to inclined extrusion of the HP–LT metamorphic rocks along the Zagros accretionary prism, Iran. Journal of Structural Geology 31, 691–706.
Sarkarinejad, K., Samani, B., Faghih, A., Grasemann, B., Moradipoor, M., 2010. Implications of strain and vorticity of flow analyses to interpret the kinematics of an oblique convergence event (Zagros Mountains, Iran). Journal of Asian Earth Sciences 38, 34–43.
Sheikholeslami, M.R., Pique, A., Mobayen, P., Sabzehei, M., Bellon, H., Hashem Emami, M., 2008. Tectono-metamorphic evolution of the Neyriz metamorphic complex, Quri-Kor-e-Sefid area (Sanandaj-Sirjan Zone, SW Iran). Journal of Asian Earth Sciences 31, 504–521.
Simpson, C., 1981. Ductile shear zones: a mechanism of rock deformation in the orthogneisses of the Maggia Nappe, Ticino. PhD thesis, ETH Zurich.
Srivastava, H.B., Hudleston, P., Earley III, D., 1995. Strain and possible volume loss in a high-grade ductile shear zone. Journal of Structural Geology 17, 1217–1231.
Stocklin, J., 1968. Structural history and tectonics of Iran. A review. American Association of Petroleum Geologists Bulletin 52, 1229–1258.
Takin, M., 1972. Iranian geology and continental drift in the Middle East. Nature 235, 147–150.
Talbot, C.J., 1970. The minimum strain ellipsoid using deformed quartz veins. Tectonophysics 9, 47–76.
Talbot, C.J., 1987. Strains and vorticity beneath a tabular batholith. Tectonophysics 138, 123–158.
Talbot, C.J., Sokoutis, D., 1995. Strain ellipsoids from incompetent dykes: application to volume loss during mylonitization in the Singö gneiss zone, central Sweden. Journal of Structural Geology 17, 927–948.
Truesdell, C., 1953. Two measures of vorticity. Journal of Rotational Mechanical Analysis 2, 173–217.
Twiss, R.J., Moores, E.M., 1992. Structural Geology. W.H. Freeman and Company, New York, pp. 532.
Vitale, S., Mazzoli, S., 2008. Heterogeneous shear zone evolution: the role of shear strain hardening/softening. Journal of Structural Geology 30, 1383–1395.
Xypolias, P., 2009. Some new aspects of kinematic vorticity analysis in naturally deformed quartzites. Journal of Structural Geology 31, 3–10.